Asociación Argentina
de Mecánica Computacional

Mecánica Computacional Vol XXXVII, págs. 139-148 (artículo completo)
A. Cardona, L. Garelli, J.M. Gimenez, P.A. Kler, S. Márquez Damián, M.A. Storti (Eds.)
Santa Fe, 5-7 Noviembre 2019

EVALUATION OF STATIC DAMAGED ROPE RESPONSE BASED ON CABLE-BEAM ELEMENT FORMULATION

Juan F. Beltran[a,b] **and Tomás Bravo**[b]

[a]*Associate Professor, Dept. of Civil Engineering, University of Chile, Blanco Encalada # 2002 Of. 440, Santiago, Chile. E-mail: jbeltran@ing.uchile.cl*

[b] *Graduate Student, Dept. of Civil Engineering, University of Chile, Blanco Encalada # 2002, Santiago, Chile. E-mail: tomas.bravo@ing.uchile.cl*

Keywords: Damage, rope failure, cable-beam element, finite element algorithm.

Abstract. In this paper a numerical model to evaluate the static response of damaged ropes is presented. In this study, damage corresponds to the complete rupture of one or more rope components in a particular rope cross-section. In particular, the proposed model couples the effects of two phenomena that rule damaged rope response: strain localization and asymmetry in damage distribution. The proposed model relies on the finite element method in which the damaged rope is discretized along its length into 1D two-noded nonlinear cable-beam elements with six degrees of freedom (dof) per node and Bernoulli´s kinematic hypothesis. These elements account for the helical structure of a rope (cable) as well as the axial-bending, axial-torsional, and bending-torsional interactions. Experimental static tensile test data reported in the literature of homogeneous ropes with nonlinear constitutive laws and overall diameters that range from 6 mm to 147 mm are used to validate the proposed model. Tested ropes are damaged at ropes midspan location with damage levels (percentage of the broken components of the damaged cross-section with respect to the intact rope) symmetrically and asymmetrically distributed on rope cross-sections that vary from 5% to 55%. Comparison results indicate that the proposed model accurate predicts the static response of damaged ropes, considering a wide range of rope diameter and damage level values, achieving numerical robustness and computational efficiency.

1 INTRODUCTION

Ropes experience damage throughout their loading history and from continued aggression of the environment (urban, industrial, marine, etc.). Damage to ropes degrades rope components properties, process that may induce the partial or complete rupture of some of the rope components, and eventually, compromise the safety and integrity of the structural system that the damaged ropes are part of. Hence, the understanding of the effects of damage on the mechanical behavior of ropes is essential to estimate rope service life at the design stage and to establish the appropriate rope inspection methods and discard criteria (Chaplin, 2005).

Previous researches (MacDougall and Barlett, 2006; Ward et al., 2006; Beltran and De Vico, 2015; and Beltran et al., 2018 among others) have shown that two of the main mechanisms that govern the response of damaged ropes are strain localization and asymmetry in damage distribution, in which bending deformation takes place in ropes due to the latter mechanism; thus, ropes eventually undergo changes in curvature. Under this condition, a flexible model (rope treated as a fiber element, i.e., slender body of negligible bending and torsional stiffness) is inadequate to accurately describe the mechanical behavior of the damaged rope. In this kind of problem, a richer model for the rope should be developed in which axial, torsion, and bending strains as well as axial-bending, axial-torsion, and bending-torsion interactions need to be accounted for (the so-called stiff cable model) (Luongo and Zulli, 2013).

In this paper a robust and computational efficient numerical model that couples the effects of strain localization and asymmetry in damage distribution on the static response of damaged ropes is presented. The proposed model relies on the finite element method in which the damaged rope is discretized along its length into 1D two-noded nonlinear cable-beam elements with six degrees of freedom (dof) per node and Bernoulli´s kinematic hypothesis. These elements account for the helical structure of a rope (cable) as well as the axial-bending, axial-torsional, and bending-torsional interactions. Experimental static tensile tests data reported in the literature on polyester ropes and metallic strands (diameters vary from 6 mm to 166 mm) asymmetrically damaged (initial cross-section damage level varies from 5% to 55%) are used for validation purposes and also to interpret them based on the simulations provided by the proposed model.

2 NUMERICAL ALGORITHM FOR THE ANALYSIS OF DAMEGED ROPES

In this section, the proposed numerical algorithm that relies on the nonlinear finite element method considering the updated Lagrangian formulation is outlined. Hereafter, the proposed numerical model is termed *NLCBM*.

Considering a generic straight prismatic two-noded cable-beam element b of length L_b depicted in Fig. 1. The element has a total of twelve degrees of freedom (dofs), in which x denotes the longitudinal axis and (y, z) the two principal axes of the cross-section. The displacements of a standard uniaxial two-noded cable-beam element in a 3D-space consist of three translation u, v, and w in x, y, and z directions, and three rotations θ_x, θ_y, and θ_z, around axes x, y, and z respectively, which are functions of the position x along the element. Along the kinematic variables previously mentioned, their corresponding nodal forces are also depicted in the figure for both nodes (node I and J), in which F_r and M_q refer to a force in the r direction and a moment around the q direction respectively.

It is assumed that the generic cable-beam element obeys the Euler-Bernoulli kinematic hypothesis. As such, the displacements $\{u^m\}(x,y,z)$ of a material point m with coordinates (y,z) at a section with distance x from the origin of the reference frame, that describe the rigid body motion of the section plane, are given by the following expressions

$$u_t^m(x,y,z) = \Big(u(x) - y\theta_z(x) + z\theta_y(x)\Big)\cos\beta^m + \sqrt{z^2+y^2}\,\theta_x(x)\sin\beta^m \quad (1a)$$

$$u_y^m(x,y,z) = v(x) - z\theta_x(x) \quad (1b)$$

$$u_z^m(x,y,z) = w(x) + y\theta_x(x) \quad (1c)$$

where u_t^m corresponds to the displacement in the t direction of the material point m that is part of a fiber oriented in an angle β relative to the x axis. In this way, the orientation of the rope components, that in their initial configurations correspond to a circular helix curve, that form the rope are accounted for (Fig. 1). The transverse displacements u_y^m and u_z^m of the material point m are assumed to be small based on previous works on asymmetrically damaged ropes (Beltran and De Vico, 2015; and Beltran et al., 2018); thus, the same transverse displacements of a fiber aligned along the longitudinal axis of the rope are considered for the case of a fiber inclined relative to the latter due to its initial helical geometry along with neglecting their contributions to u_t^m. In the above expressions, it is important to point out that the following kinematic relations hold: $\theta_z(x) = \mathrm{d}v(x)/\mathrm{d}x$ and $\theta_y(x) = \mathrm{d}w(x)/\mathrm{d}x$, where $\mathrm{d}(\cdot)/\mathrm{d}x$ is the first derivative operator acting on the corresponding function.

Rope components are assumed to behave as fiber elements; as such the only term of the updated Green strain increment tensor accounted for the computation internal virtual work in Eq. (3) is given by

$$\varepsilon_{tt}^m = \frac{\partial u_t^m}{\partial t} + \frac{1}{2}\left[\left(\frac{\partial u_t^m}{\partial t}\right)^2 + \left(\frac{\partial u_y^m}{\partial t}\right)^2 + \left(\frac{\partial u_z^m}{\partial t}\right)^2\right] \quad (2)$$

where u_t^m, u_y^m, and u_z^m are the displacement fields given by Eqs (1).

It is important to point out that the displacement and rotation functions $u(x)$ and $\theta_p(x)$ (p = x, y, and z) respectively, depend on the variable x (longitudinal axis of the rope); thus, computation of the derivatives with respect to t (local longitudinal axis of the rope components) in the above equation, gives rise to the terms $\cos\beta$, $\cos^2\beta$, $\cos^3\beta$, $\cos^2\beta\sin\beta$, and $\sin\beta\cos\beta$ in the expression for ε_{tt}^m due to the helical nature of the rope components. Therefore, the expression for ε_{tt}^m in terms of the derivatives with respect to x is given by

$$\varepsilon_{tt}^m = \frac{\partial u_t^m}{\partial x}\cos\beta^m + \frac{1}{2}\left[\left(\frac{\partial u_t^m}{\partial x}\right)^2 + \left(\frac{\partial u_y^m}{\partial x}\right)^2 + \left(\frac{\partial u_z^m}{\partial x}\right)^2\right](\cos\beta^m)^2 \quad (3)$$

Following the notation proposed by Yang and Kuo (1994), the principal of virtual works in an incremental form yields

$$\int_{V_{j-1}} (E_t)_{j-1}\Delta e_j \delta_{j-1} e dV_{j-1} + \int_{V_{j-1}} \sigma_{j-1}\delta_{j-1}\eta dV_{j-1} = F_{j-1}^{j} - F_{j-1}^{j-1} \quad (4)$$

where e, and η correspond to the linear and nonlinear terms of the updated Green strain tensor respectively and Δe_j is the increment of the linear term for the *j-th* step of the analysis; $(E_t)_{j-1}$, V_{j-1}, and σ_{j-1} are the tangent modulus, the volume of the component over which energy is

computed, and the normal axial stress in the j-1 step of the analysis respectively; the operator $\delta_{j\text{-}1}$ refers to a virtual variation of the variable operated upon based on the (j-1) configuration. The right-hand side of the above equation ($F_{j\text{-}1}{}^{j}$ and $F_{j\text{-}1}{}^{j\text{-}1}$) denote the virtual work done bythe external loads (surface tractions and body forces) acting on the body at j and (j-1) configurations respectively.

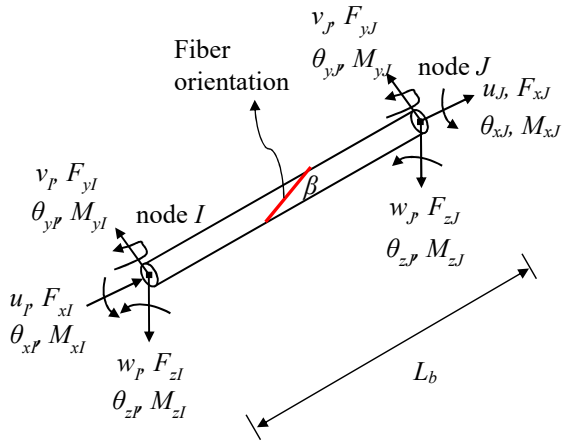

Figure 1.Generic two-noded stiff cable-beam element b in a 3D-space.

By utilizing a standard finite element procedure, the virtual work equation (Eq. 4), applied to a generic element b that is part of the rope discretization, can be turned into an incremental algebraic equation for the generic element from the step of the analysis j-1 to j as

$$([k_L] + [k_G])^{j-1}_{j-1,b}\{du\}^{j}_{j-1,b} = \left(f^{j}_{j-1} - f^{j-1}_{j-1}\right)_b \tag{5}$$

where $[k_L]_b$ and $[k_G]_b$ are the local linear and geometric stiffness matrices of element b, respectively; $\{u\}_b$ increment in nodal displacement vector of element b; and $(f_{j\text{-}1}{}^{j} - f_{j\text{-}1}{}^{j\text{-}1})_b$ is the increment in nodal forces vector from the step of the analysis j-1 to j of element b, in which both quantities are referred to the deformed configuration of the element b related to j-1 step of the analysis. Following the procedure established by Yang and Kuo (1994) and using Eq. (4), the aforementioned stiffness matrices and nodal load vector can be derived using for the trial kinematic variables functions $v(x)$, $w(x)$, $\theta_z(x)$, and $\theta_y(x)$ and their corresponding virtual forms correspond to the well-known Hermite cubic polynomials and for the case of $u(x)$ and $\theta_x(x)$ linear interpolations functions are used for trial and virtual ones. Details of the computations of the aforementioned entities can be found in Beltran and Bravo (2019).

Beltran and De Vico (2015) established that the effect of asymmetric damage distribution on ropes can be represented by unbalanced sinusoidal loads (q_y and q_z) acting in two perpendicular (principal) planes (i.e., rope subjected to biaxial bending). As such, in the proposed finite element algorithm-based, nodal forces P_i, and Q_i associated to q_z and q_y are given by

$$\{Q\}_b = \int_{L_b}\left[N_{\theta_z}\right]^T q_{y,b}\,d\xi;\;\; \{P\}_b = \int_{L_b}\left[N_{\theta_y}\right]^T q_{z,b}\,d\xi \tag{6}$$

where the row vectors $[N_{\theta z}]$ and $[N_{\theta y}]$ correspond to the Hermite cubic polynomials functions used to approximate $v(x)$, $w(x)$, $\theta_z(x)$, and $\theta_y(x)$ (Fig. 1); superscript T refers to the transpose operator; and subscript b refers to a generic cable-beam element. The corresponding nodal forces are depicted in Fig. 1 with their corresponding dof. Expressions for q_y and q_z for different rope constructions types are given by Beltran and De Vico (2015) and Beltran et al. (2017).

The finite element-based model proposed to study damaged rope response, relies on the ability of broken rope components to carry their proportionate share of axial loads over a distance measured from the failure region, which is referred as the *recovery length* (*rl*) (Raoof, 1991). Along this length, the model accounts for the potential continuous increment of the contribution to damaged rope response of the broken components along with the fact that the asymmetry of the rope cross-section is diminished. As long as the broken rope components do not fully develop their recovery length values, the formulation of the proposed model accounts for the strain localization and asymmetry in damage distribution, as well as their interactions, effects on rope response.

According to Beltran and Williamson (2010), the recovery length value (*rl*) of a helical broken rope component can be estimated as

$$rl = \frac{1}{\mu C_2} \ln\left[\frac{\mu C_2 T_s}{C_1} + 1\right] \tag{7}$$

where a Coulomb friction model is considered in which T_s is the tension in the broken rope component; μ is the friction coefficient; C_i (i = 1,2) are constants related to the normal force acting on such components whose values are discussed in detail in Beltran and Williamson (2010) and Beltran and Bravo (2019). For the case of a broken core (straight rope component), the recovery length can be estimated as

$$rl = \frac{T_c \cos\beta_2}{\mu n_2 g_{1,2}} \tag{8}$$

where n_2 is the number of the unbroken rope components in layer 2 that possess a helix angle β_2, and $g_{1,2}$ is the line contact force (radial force) exerted by the core on one rope component of the second layer (Beltran and Williamson, 2010).

A standard nonlinear finite element procedure is implemented to assess static damaged ropes responses. In a general case, damaged rope discretization strongly relies on the *rl* value of the rope due to the nonuniform axial strain distribution along this length which results in an axial strain localization around the fracture zone. This nonlinear finite element procedure is based on an iterative displacement control algorithm for each increment of the rope axial displacement. The incremental-iterative equation of global equilibrium in a nonlinear finite element procedure has the following form:

$$[K_{dr}]_{j-1}^{k-1}\{d\boldsymbol{u}\}_j^k = \{d\boldsymbol{Q}\}_j^k + \{\boldsymbol{R}\}_j^{k-1} \tag{9a}$$

$$[(K_L)_{dr} + (K_G)_{dr}]_{j-1}^{k-1}\{d\boldsymbol{u}\}_j^k = \{d\boldsymbol{Q}\}_j^k + \{\boldsymbol{R}\}_j^{k-1} \tag{9b}$$

where $[K_{dr}]$ is the tangent stiffness matrix of the damaged rope in which the first contribution, $(K_L)_{dr}$, is the linear stiffness and the second contribution, $(K_G)_{dr}$, is the geometric stiffness; $\{d\boldsymbol{u}\}$ increment in the displacement vector; $\{d\boldsymbol{Q}\}$ is the increment in the external load vector;

$\{\boldsymbol{R}\}$ is the residual load vector (difference between internal and external loads); and subscript j and superscript k represent the step of the analysis and the number of iterations in that step respectively. The entities $[K_{dr}]$, $\{d\boldsymbol{Q}\}$, and $\{\boldsymbol{R}\}$ are referenced to a fixed global coordinate system and they are obtained utilizing standard assembly procedures for the damaged rope stiffness and load vectors.

As previously commented, as asymmetry of rope cross-section diminishes along the recovery length, the unbalanced transverse sinusoidal loads get smaller in magnitude as well; hence, strain localization and asymmetry in damage distribution phenomena have less influence on rope response toward rope ends as depicted in Fig. 2. The numerical algorithm implemented to solve Eqs. 9 and the procedure to compute the nodal forces are explained in detail in Beltran and Bravo (2019).

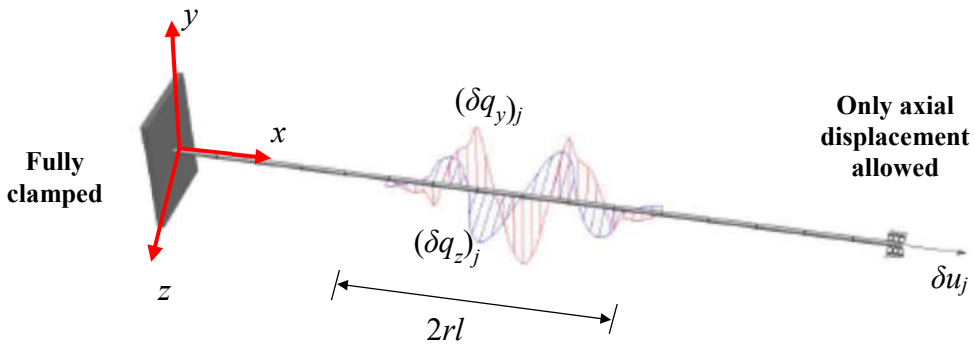

Figure 2. Damaged rope discretized into two-noded stiff cable-beam elements

3 EXAMPLES OF ESTIMATES OF DAMAGED ROPE RESPONSE

In Fig. 3 the analysis of the response of a small-scale polyester rope is presented based on the results provided by *NLCBM*, whose results are validated with the one given by 3D FE simulations (Beltran and Vargas, 2012). Rope´s diameter is equal to 6 mm and five out of nine rope components are initially cut prior testing to rupture (colored black). Hence, 55% of the cross-section is initially damaged in which damage has a symmetric distribution (Fig. 3); thus it is expected that the strain localization phenomenon rules rope response. The core (central straight rope component) is the only broken component that develops a finite recovery length value because is confined by the unbroken rope components of the second layer of the rope. Rope specimen has length (L) equal to 610 mm (approximately $8p$, p is the pitch distance) and based upon Eq. 8, the recovery length value of the broken core of the rope analyzed is 220 mm. This value was computed assuming a friction coefficient equal to 0.1 (Beltran and Vargas, 2012), contact between rope components only in the radial direction, and a small level of rope deformation (10% of the specified failure axial strain).

In Fig. 3a the axial strains of the central node of the core of the rope analyzed are plotted at different positions along the rope length (x variable) from the rupture zone for different levels of rope axial strain. The x variable is normalized by one half of the rope length ($L/2$) due to symmetry of the results obtained where the parameter $x/L/2$ equal to 1 corresponds to the fractured zone (rope midspan) and $x/L/2$ equal to 0 corresponds to one end of the rope. Results plotted in this figure indicate that strains are maximum at $x/L/2=1$ inducing a strain localization zone and start decreasing ,due to the transferring of axial load from the unbroken

components to the broken core by friction, until the recovery length of the broken core is fully developed(constants strain values). Along *rl*, five two-noded cable-beam elements are used to capture the strain localization phenomenon, and according the results shown in Fig. 3a, the recovery length value is well estimated by Eq. 8 as well as the axial strain values developed in this region (relative to the results given by the 3D FE models) in which the average maximum value is about 25% greater than the ones outside of this region.

In Fig. 3b, capacity curves estimated by *NLCBM* and 3D FE compare quite well between each other although the former overestimate the residual strength and deformation capacity in 15% and 10% respectively relative to the 3D FE results. Experimental data for this rope specimen, agree with predicted values only for small rope axial strain values (less than 0.025). For greater strain values, experimental data gets more flexible than the predicted one due to the progressive damage, and eventually failure, of some of the rope components around rope terminations as commented by Li et al (2002).

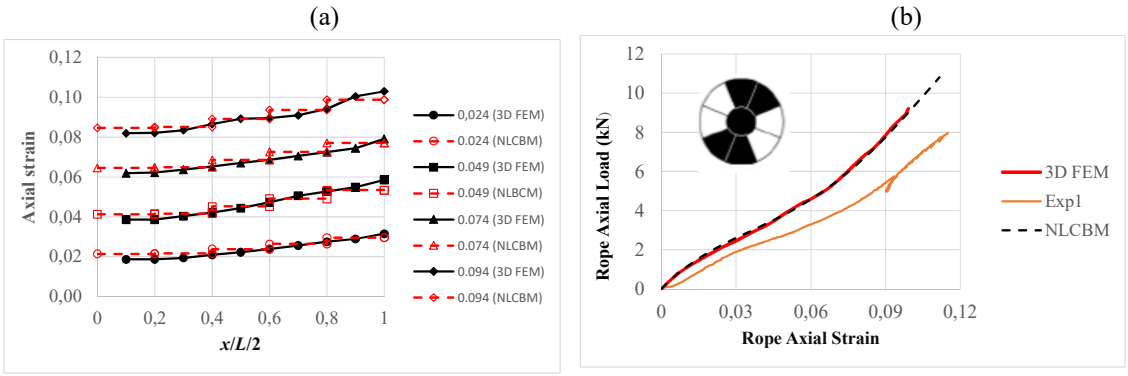

Figure 3. (a) Strain distribution along the broken core; (b) capacity curves: measured and predicted (*NLBM* and 3D FEM) values for a rope with initial damage of 55%.

The estimated and measured response of a 19.9 mm diameter aluminium damaged strand is presented in Fig. 4. The damage is asymmetrically distributed on strand surface (two out of nineteen wires broken); thus, according to Beltran et al (2018), asymmetric damage distribution governs damaged strand response. Axial strains developed by unbroken wires were measured using strain gauges (S.G.) and despite of some local nonlinear response of the measured strain values, especially for low values of axial load, both measured and predicted (ES-W*i* in Fig. 4a) values suggest that a gradient in axial strain distribution is developed in which greater strains take place adjacent to damage and smaller strains opposite to damage (Fig. 4a). The ratio values between the maximum and minimum strains are 1.85 and 1.6 for the measured and estimated cases respectively. In addition, relative to the virgin simulation (undamaged strand), ratio values for the minimum and maximum cases are [0.72, 0.74] and [1.33, 1.18] for the measured and estimated cases respectively.

Regarding the capacity curves presented in Fig. 4b, measured and estimated (*NLBCM* and 3D FEM) curves are compared for both virgin and damaged strand cases. In particular, *NLCBM* underestimates the measured strength capacity of virgin and damaged strand in 13%, accurately predicts virgin deformation capacity and overestimates in 8% this value for the damaged case. In terms of the elastic stiffness, *NLCBM* model slightly overestimates the virgin measured value (1.5%) and in 7% the average measured one. 3D FEM provides similar results to the ones given by *NLCBM* that were previously discussed but with a higher computational cost involved.

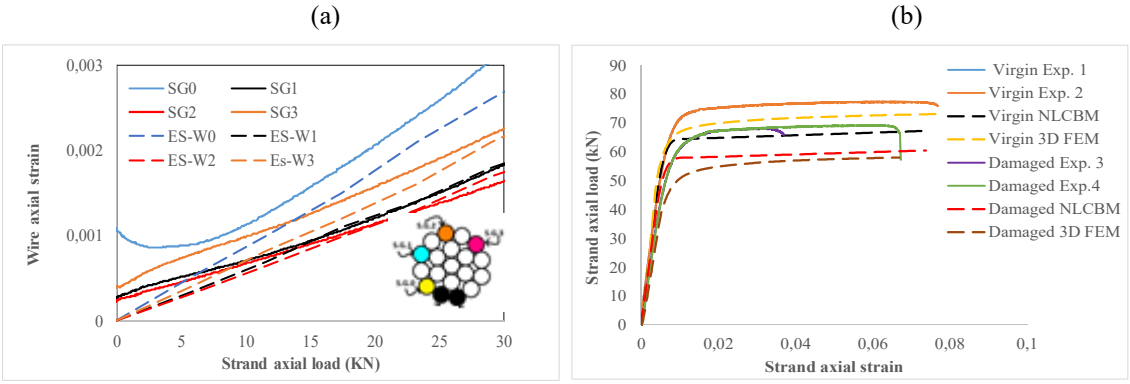

Figure 4. (a) Axial strain distribution on damaged strands cross-section and (b) capacity curves: measured and predicted (*NLBM* and 3D FEM) values

Asymmetry in damage distribution also induces a lateral deflection in the damaged strand (Fig. 5a). To validate the *NLCBM*, the waviness of two commercial steel strands (diameters equal to 3.5mm and 22.2 mm) is studied using the proposed model and 3D FEM with one (1-D), two (2-D) and six (6-D) wires cut in their linear regime responses (Fig. 5). The results presented by both numerical models compare quite well between each other in which the values predicted by the *NLBM* are in the range of [-15%,+12%] relative to the ones predicted by the 3D FEM (Fig. 5b,c).

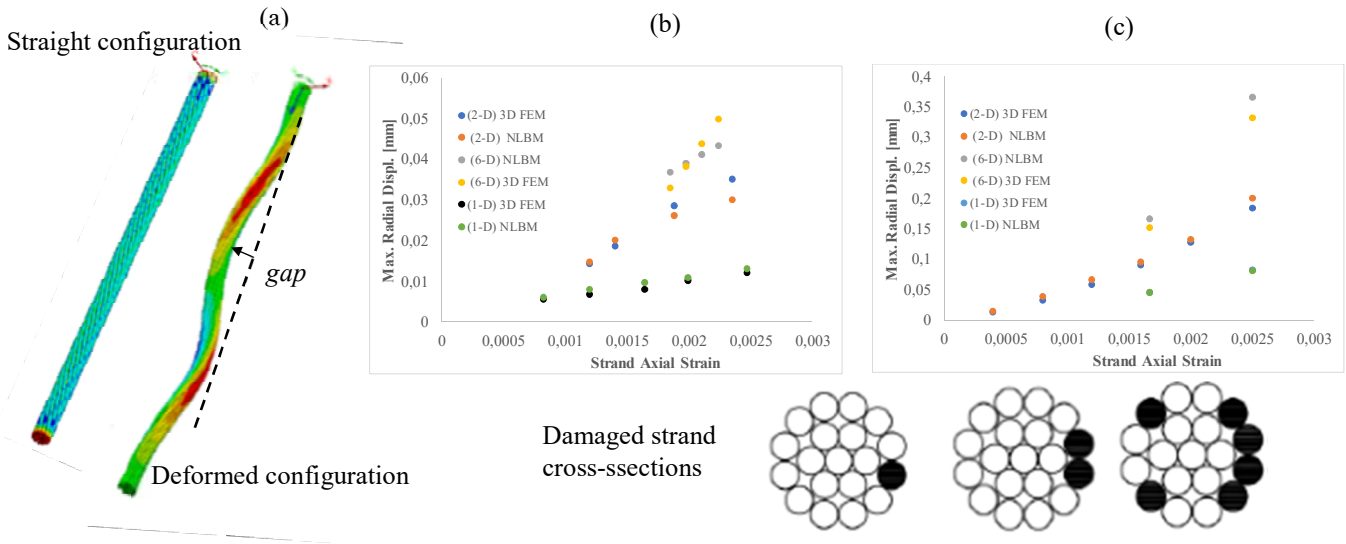

Fig.5. (a) Sketch of the initial and deformed configuration of asymmetrically damaged strand; (b) and (c) maximum radial displacement for a 3.5mm and 22.2 mm diameter asymmetrically damaged strands respectively.

The discard criteria specified by ISO 4309 (2010) for a damaged strand related to strand waviness, established that the *gap* between a straightedge and the underside of the helix (Fig. 5a) should not be greater than 1/3*d* or 1/10*d*, being *d* the diameter of the strand, if the strand never runs through a sheave or spools on to the drum or if it does respectively. For the examples presented in this study, the maximum radial displacement values for the 3.5 mm and 22.2 diameter strands are 1.4% and 1.7% of their diameter values respectively, considering in both cases six wires cut (6-D), values that are lower than the two

aforementioned critical values. Hence, asymmetry in damage distribution slightly perturbs initial straight strands configuration.

Lastly, the analysis of the static response of a polyester jacketed rope with parallel sub-ropes construction with specified breaking stress equal to 700 tonnes (6865 kN) is presented in Fig. 6. Rope´s diameter is equal to 147 mm and the rope has 20 sub-ropes in which each sub-rope is built by twisting three strands together. The initial damage inflicted to cross-section was set to 10% and the ratio L/d is equal to 40 (Ward et al., 2006); thus, considering that the recovery length of the broken strands was estimated in 2950 mm (Eq. 7) due to the jacket confinement (Beltran and Bravo, 2019), rope´s length is not long enough to allow them to fully develop their recovery length values. Hence, rope cross-section does not retrieve their symmetry although transverse sinusoidal loads diminish in magnitude as approaching to the rope ends and consequently strain localization and asymmetry in damage distribution phenomena are present along the entire rope. Exp. data curve (Fig. 6a) shows some individual strand failures that soften its response prior to its complete rupture. Based on an estimate given by Beltran et al. (2017), the damage level increased to 20% distributed to five sub-ropes. After the individual strand failures occurred (strain greater than 0.05), Exp. data curve is bounded by the *SLM* (20%) and *NLCBM* (20%) in a narrow region in which the latter lies in the solution space and underestimates the measured residual strength and deformation capacity in 6% and 3% respectively (Fig. 6b), in which *SLM* solely accounts for the strain localization phenomenon (Beltran et al., 2017). For low strain values (less than 0.025), Exp. data curve matches well with the *ADDM* (10%) curve (solely accounts for the asymmetric damage distribution phenomenon), after which the former experiences a stiffening process which results in a slightly stiffer response than the upper bound curve (*SLM*) that ends up with the individual strand failures previously commented.

In Fig. 6b, the deformed configuration of the rope for two levels of axial strain (0.021 and 0.062) is depicted. Results indicate that the maximum lateral deflection located at rope midspan is equal to 0.5% and 1.3% of the rope´s diameter (147 mm) respectively. Rope deflection, which is basically an inclined helix with decreasing amplitude, slightly perturbs the initial rope straight configuration.

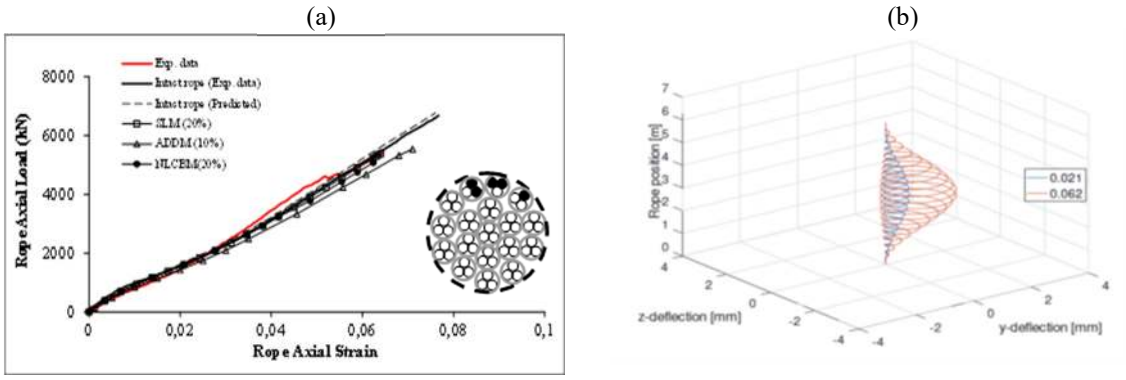

Figure 6. (a) Capacity curves and (b) deformed configurations of initially damaged rope with SBS equal to 700tonnes

4 FINAL REMARKS

In this paper, the response of damaged polyester ropes and metallic strands whose diameter values range from 3.5 mm to 147 mm with a wide variety of damage levels were studied. To this end, a finite element-based procedure that couples the effects of strain localization and

asymmetry in damage distribution on damaged rope response was used. For analysis purposes, damaged ropes/strands were discretized along their lengths into uniaxial two-noded nonlinear cable-beam elements with six degrees of freedom (dof) per node and Bernoulli´s kinematic hypothesis. The proposed generic cable-beam element accounts for the helical structure of a rope (cable) as well as the axial-bending, axial-torsional, and bending-torsional interactions.

Comparisons with experimental data and simulations from 3D FEM indicate that the proposed algorithm is capable of accurately predicting damaged rope/strand response that includes capacity curve, axial strain field along rope´s length, and deformed configuration. In addition, the proposed algorithm seems to be a promising computational tool to estimate damaged rope/strand response and interpret and extend experimental data due to its robustness and computational efficiency since most of the simulations were obtained in less than five minutes on a standard multi-core processor laptop (Intel Core i7-16 Gb RAM). Despite the good performance shown by the proposed algorithm, additional comparisons with other well-accepted numerical technique (e.g. 3D FEM) and experimental data of ropes/strands comprised of diverse materials and construction types are needed to establish the range of applicably of this algorithm.

REFERENCES

Beltran, J.F. and Williamson, E. Numerical simulation of damage localization in polyester mooring ropes. *Journal of Engineering Mechanics*, 136 (8): 945-959, 2010.

Beltran, J.F. and De Vico, E. Assessment of static rope behavior with asymmetric damage distribution. *Engineering Structures*, 86: 84-98, 2015.

Beltran, J.F., Ramirez, N., and Williamson, E. Simplified analysis of the influence of strain localization and asymmetric damage distribution on static damaged polyester rope behavior. *Ocean Engine*ering 145: 237-249, 2017.

Beltran, J.F., Nuñez, E., Nuñez, F., Silva, I., Bravo, T., and Moffat, R. Static response of asymmetrically damaged metallic strands: Experimental and numerical approach. *Construction and Building Material*, 192: 538-554, 2018.

Beltran, J.F. and Bravo, T. Evaluation of the coupled effect of strain localization and asymmetric damage distribution on rope response: Numerical approach based on a nonlinear cable-beam element. *Engineering Structures* (under review), 2019.

Chaplin, C.R. The fatigue and degradation mechanisms of hoisting ropes. In: Hoist and Haul Conference, Perth, Australia, 359-366, 2005.

Li D., Miyase A., Williams J.G., and Wang S.S. Damage tolerance of synthetic- fiber mooring ropes: small-scale experiments and analytical evaluation of damaged subropes and elements. Technical report, CEAC-TR-03-0101, University of Houston, 2002.

Luongo, A. and Zulli, D. *Mathematical models of beams and cables*. Wiley & Sons, Inc., NJ, USA, 2013.

MacDougall, C. and Bartlett, F. Mechanical model for unbonded seven-wire tendon with single broken wire. *Journal of Engineering Mechanics*, 132 (12):1345-1353, 2006.

Raoof, M. Wire recovery length in a helical strand under axial fatigue loading. *International Journal of Fatigue*, 13:127-132, 1991.

Ward, E.G., Ayres, R., Banfield, S., and O`Hear, N. Full scale experiments on damaged polyester rope. Technical report, JIP-FP-1, Offshore Technology Research Center, 2006.

Yang, Y.B. and Kuo, S.R. *Theory and Analysis of Nonlinear Framed Structures*, first ed. Prentice Hall, Singapore, 1994.